Localized two-vibron bound-state dynamics in a molecular lattice with a defect: Resonances between bound, localized, and free states

V. Pouthier*

Laboratoire de Physique Moléculaire, UMR CNRS 6624, Faculté des Sciences—La Bouloie, Université de Franche-Comté, 25030 Besançon cedex, France

The two-vibron dynamics in a molecular nanowire with a local defect is characterized. The integration of the time dependent Schrodinger equation has revealed the occurrence of two singular behaviors. When the defect frequency shift is close to the intramolecular anharmonicity, a resonance between the localized two-vibron bound state and the two-vibron free states continuum takes place. The resonance breaks the localized vibron pair and two independent vibrons are emitted on each side of the defect so that an exponential decay of the defect vibrational population occurs. By contrast, when the defect frequency shift is almost twice the anharmonicity, a resonance occurs between the localized two-vibron bound state and the continuum formed by a vibron trapped on the defect and a second vibron delocalized along the nanowire. In that case, the trapped vibron enhances the hopping constant experienced by the second vibron near the defect so that two localized states occur in which the two vibrons are trapped around the defect. Due to the superimposition of these two localized states, the vibrational population is strongly localized around the defect and exhibits oscillations similar to that occurring in a classical discrete breather.

I. INTRODUCTION

Since the pioneer works of Davydov devoted to the vibrational energy flow in proteins,[1] the nonlinear dynamics of classic lattices was studied in numerous theoretical papers. In this context, the formation of intrinsic localized modes, or discrete breathers, has been the subject of intense theoretical research during the last decade (for a recent review, see for instance Refs. 2–4). Discrete breathers, which correspond to highly localized vibrational excitations in anharmonic lattices, do not require integrability for their existence and stability. They are not restricted to one-dimensional lattices and it has been suggested that they should correspond to quite general and robust solutions.[5] Since discrete breathers yield a local accumulation of the energy which might be pinned in the lattice or may travel through it, they are expected to be of fundamental importance for both energy storage and transport. Unfortunately, in spite of the great interest that breathers have attracted, no clear evidence has yet been found for their existence in real molecular lattices.

By contrast, bound states involving two high frequency vibrational excitons, also called vibrons, have been observed in several molecular structures. In that case, the intramolecular anharmonicity breaks the vibron independence and favors the formation of bound states.[6–13] A bound state corresponds to the trapping of the two quanta over only a few neighboring molecules with a resulting energy which is less than the energy of two quanta lying far apart. The lateral interaction yields a motion of such a state from one molecule to another, thus leading to the occurrence of a delocalized wave packet with a well-defined momentum. Since two-vibron bound states (TVBS) are the first quantum states which experience the nonlinearity, they can be viewed as the quantum counterpart of breathers or solitons.[8] The formation of TVBS was observed in molecular adsorbates such as H/Si(111),[14,15]

H/C(111),[16] CO/NaCl(100),[17] and CO/Ru(001)[18–22] using optical probes. Bound states in the system H/Ni(111) were investigated via high resolution electron energy loss spectroscopy.[23] Moreover, a recent experiment based on femtosecond infrared pump-probe spectroscopy, has clearly established the existence of TVBS in α-helix proteins.[24]

In a series of recent papers, it has been suggested that vibrons, and especially TVBS, could provide an alternative to the electronic transport in adsorbed molecular nanowires.[9–11,25,26] Following this idea, the present work addresses a new question related to the influence of a local defect on the two-vibron dynamics with a special emphasis on the mechanism responsible for energy localization/delocalization.

In an adsorbed nanostructure, a defect can be created by using a scanning tunneling microscope (STM). Indeed, it has been shown by Avouris and co-workers[27–30] that even under normal operating conditions, the electric field in the STM-substrate junction is high, i.e., typically of about 0.1–0.5 V/Å. This field is comparable to the internal fields that electrons experience inside atoms and molecules so that it can cause significant changes in the local electronic structure and bonding. In particular, the authors have shown that the vibrational frequency of some molecule-surface stretching modes strongly depends on the applied bias voltage between the STM and the sample. As a consequence, in a nanowire, the molecule located under the STM tip behaves as a local defect exhibiting a frequency shift when compared with the frequency of the other molecules. Therefore, the STM provides a powerful tool to control the strength of the defect frequency shift simply by tuning the bias voltage between the STM and the substrate.

In that context, it is well-known that a defect breaks the translational invariance of the nanowire and favors the occurrence of a localized state when a single vibron is excited.

This state, which is located below or above the single vibron band depending on the sign of the shift, disappears when this frequency shift is set to zero. When two vibrons are excited, the physics is more elaborate because of the various kinds of states involved in the dynamics. Indeed, in addition to two-vibron bound states and two-vibron free states (TVFS), which appears naturally in a perfect anharmonic lattice, the defect is responsible for the occurrence of a localized two-vibron bound state (LTVBS) in which the two vibrons are trapped on the defect. In addition, it allows for states in which a single vibron is localized, i.e., a localized single vibron state (LSVS), whereas the second vibron is delocalized according to a continuum of single vibron free states (SVFS). Therefore, in marked contrast with the single vibron dynamics, we expect resonances between these different two-vibron states so that the vibrational energy could be either localized or delocalized, even for a nonvanishing frequency shift of the defect.

The present paper is thus organized as follows. In Sec. II, the model Hamiltonian describing the vibron dynamics in a molecular nanowire is first introduced. Then, the time dependent two-vibron Schrodinger equation is established within the number states method. In Sec. III, the simulation of the Schrodinger equation is performed and the numerical results are presented. These results are finally discussed and interpreted in Sec. IV.

II. MODEL HAMILTONIAN AND TWO-VIBRON DYNAMICS

To model the vibron dynamics in a rather simple way, let us consider a set of N molecules adsorbed on the surface of a well-organized substrate. These molecules form a 1D lattice where the site position is denoted as $n=1,2,\ldots,N$. We thus assume that each molecule n behaves as a high frequency internal oscillator described by the standard vibron operators b_n^+ and b_n. The intramolecular anharmonicity of each molecule is taken into account according to the model of Kimball *et al.*[6] so that the resulting Hamiltonian H is essentially a Bose version of the Hubbard model with attractive interactions, as (using the convention $\hbar=1$)

$$H = \sum_n (\omega_0 + \Delta \delta_{nn_0}) b_n^\dagger b_n - A b_n^{\dagger 2} b_n^2 + J[b_n^\dagger b_{n+1} + \text{h.o.}]. \quad (1)$$

In Eq. (1), h.o. denotes the Hermitian operator, ω_0 stands for the internal frequency of each molecule, A is the positive anharmonic parameter and J represents the vibron hopping constant between nearest neighbor admolecules. The defect, located onto the n_0th site, corresponds to a molecule which the internal frequency exhibits a shift Δ with respect to the other molecules. Note that long range lateral interactions may affect the vibron dynamics but these effects are expected to be rather weak in a 1D lattice.

To characterize the two-vibron dynamics, the corresponding time dependent Schrodinger equation has to be solved. Since the Hamiltonian H [Eq. (1)] conserves the number of vibrons, this can be achieved by using the number states method[8] which was successfully applied to molecular adsorbates[9–11] and α-helix proteins.[12,13] Within this method,

the two-vibron wave function is expanded as

$$|\Psi(t)\rangle = \sum_{n_1, n_2 \geqslant n_1} \Psi(n_1, n_2, t) |n_1, n_2\rangle, \quad (2)$$

where $\{|n_1, n_2\rangle\}$ denotes a local basis set normalized and symmetrized according to the restricting $n_2 \geqslant n_1$ and where a particular vector $|n_1, n_2\rangle$ characterizes two vibrons located onto the sites n_1 and n_2, respectively. This basis set generates the entire two-vibron subspace which the dimension $N(N+1)/2$ represents the number of ways for distributing two indistinguishable quanta onto N sites.

In this context, the time dependent Schrodinger equation depends on the nature of the basis vectors involved. Indeed, when the two vibrons are far apart and far from the defect, i.e., when $n_1 \neq n_2 \neq n_0$, the Schrodinger equation is expressed as

$$i \frac{\partial \Psi(n_1, n_2, t)}{\partial t} = J[\Psi(n_1 + 1, n_2, t) + \Psi(n_1 - 1, n_2, t)]$$
$$+ J[\Psi(n_1, n_2 + 1, t) + \Psi(n_1, n_2 - 1, t)]$$
$$+ 2\omega_0 \Psi(n_1, n_2, t). \quad (3)$$

When the first vibron is located on the defect whereas the second vibron is far from the defect, i.e., when $n_2 > n_1 = n_0$, the Schrodinger equation is written as

$$i \frac{\partial \Psi(n_0, n_2, t)}{\partial t} = J[\Psi(n_0 + 1, n_2, t) + \Psi(n_0 - 1, n_2, t)]$$
$$+ J[\Psi(n_0, n_2 + 1, t) + \Psi(n_0, n_2 - 1, t)]$$
$$+ (2\omega_0 + \Delta) \Psi(n_0, n_2, t). \quad (4)$$

Note that a similar equation is obtained when the second vibron is on the defect whereas the first vibron lies far from the defect, i.e., when $n_1 < n_2 = n_0$. When the two vibrons, lying far from the defect, are located on the same site, i.e., when $n_1 = n_2 \neq n_0$, the Schrodinger equation is expressed as

$$i \frac{\partial \Psi(n_1, n_1, t)}{\partial t} = \sqrt{2} J[\Psi(n_1 - 1, n_1, t) + \Psi(n_1, n_1 + 1, t)]$$
$$+ (2\omega_0 - 2A) \Psi(n_1, n_1, t). \quad (5)$$

Finally, when the two vibrons are located on the defect, i.e., when $n_1 = n_2 = n_0$, the Schrodinger equation is written as

$$i \frac{\partial \Psi(n_0, n_0, t)}{\partial t} = \sqrt{2} J[\Psi(n_0 - 1, n_0, t) + \Psi(n_0, n_0 + 1, t)]$$
$$+ (2\omega_0 + 2\Delta - 2A) \Psi(n_0, n_0, t). \quad (6)$$

Note that all the other elements of the Schrodinger equation are obtained by symmetry due to the Hermitian nature of the Hamiltonian H.

At this step, let us mention the following picture which provides an intuitive way to understand and to interpret the two-vibron dynamics. Indeed, as discussed in detail in Refs. 9–13, Eqs. (3)–(6) clearly show the equivalence between the two-vibron dynamics and the dynamics of a single fictitious particle moving quantum mechanically on the 2D lattice displayed in Fig. 1. Within this equivalence, the two-vibron
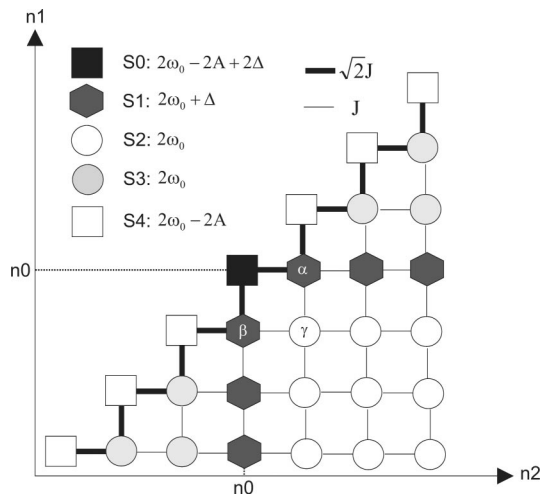
FIG. 1. 2D lattice for the equivalence between the two-vibron dynamics and the tight-binding model for a single fictitious particle (see the text).

wave function $\Psi(n_1,n_2,t)$ can be viewed as the wave function of the fictitious particle. According to Eqs. (3)–(6), its dynamics is described by a tight-binding Hamiltonian characterized by self energies located on each site and hopping matrices which couple nearest neighbor sites. Both the intramolecular anharmonicity and the presence of the defect in the real nanowire are responsible for the occurrence of defects in the 2D lattice leading to a shift of the corresponding self-energies. These defects discriminate between localized states and delocalized states for the fictitious particle, which, in turn, correspond to localized, bound or free states for the two vibrons.

As illustrated in Fig. 2, the nanowire exhibits basically four kinds of different eigenstates. The two-vibron bound states (TVBS), which refer to a localization of the fictitious particle close to the sites $n_1=n_2 \neq n_0$ (open squares in Fig. 1), form an energy band around $2\omega_0-2A$. The two-vibron free
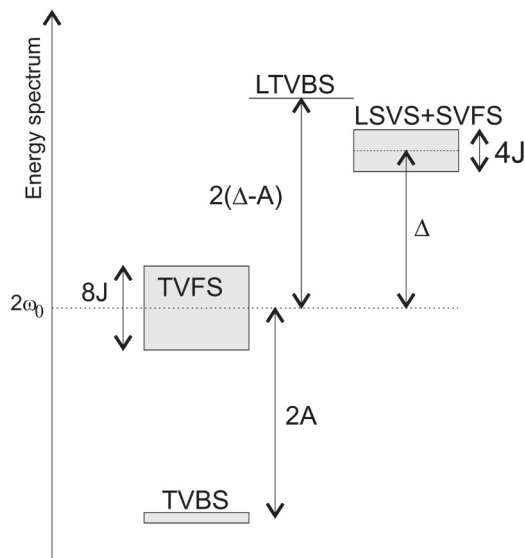

FIG. 2. Representation of the two-vibron energy spectrum in a molecular nanowire with a defect.

states (TVFS), connected to the delocalization of the fictitious particle far from the defect sites of the 2D equivalent lattice (circles in Fig. 1), form an energy continuum around $2\omega_0$. States corresponding to the localization of the first vibron and to the delocalization of the second vibron (LSVS+SVFS) correspond to the localization of the fictitious particle in the vicinity of the sites $n_1<n_2=n_0$ and $n_1=n_0<n_2$ (diamonds in Fig. 1). These states form an energy band around $2\omega_0+\Delta$. The localized two-vibron bound state (LTVBS), connected to the localization of the fictitious particle around the site $n_1=n_2=n_0$, is a discrete state located around $2\omega_0+2\Delta-2A$.

Therefore, the 2D equivalent lattice (Fig. 1) provides a helpful picture allowing a comprehensive representation of the two-vibron energy spectrum (Fig. 2). This spectrum clearly shows the ability to have resonances between the different kinds of states depending on the value taken by the frequency shift Δ. The next section is thus devoted to the characterization of these resonances through the numerical resolution of the time dependent Schrodinger equation, Eqs. (3)–(6).

III. NUMERICAL RESULTS

In this section, the numerical integration of the time dependent two-vibron Schrodinger equation is performed within the fourth order Runge-Kutta method.[31] To realize the simulation, typical values for molecular adsorbates are used for the parameters enter Eq. (1). Indeed, for small adsorbed molecules, the anharmonic parameter, usually close to the gas phase value, ranges between $10-40$ cm^{-1} whereas the vibron bandwidth is typically less than or about 10 cm^{-1}. For instance, for the CO/Ru system (see Ref. 11 and references inside), the anharmonicity is equal to $A=15.56$ cm^{-1} and the hopping constant is equal to $J=3.82$ cm^{-1}. For the H/Si(111) system, the vibron bandwidth is equal to 10 cm^{-1} and the anharmonicity was found to be $A=34$ cm^{-1}.[14] As pointed out in the Introduction, the defect frequency shift Δ is considered as a free parameter which can be controlled experimentally. Note that in the present paper we consider positive Δ values, only, and other situations will be addressed in a forthcoming work.

To understand the influence of the defect onto the two-vibron dynamics, we thus assume that the two quanta are initially located on the defect so that the two-vibron state at time $t=0$ is expressed as

$$\Psi(n_1,n_2,t=0) = \delta_{n_1,n_0}\delta_{n_2,n_0}. \qquad (7)$$

Among the different observables which can be extracted from our simulation, we essentially focus our attention on the behavior of the vibron population along the nanowire. The population represents a key observable to describe the vibrational energy flow and allows us to discriminate between both energy localization and delocalization. Therefore, in terms of the two-vibron wave function $\Psi(n_1,n_2,t)$, the population at site n and at time t, $p(n,t)=\langle\Psi(t)|b_n^\dagger b_n|\Psi(t)\rangle$, is expressed as
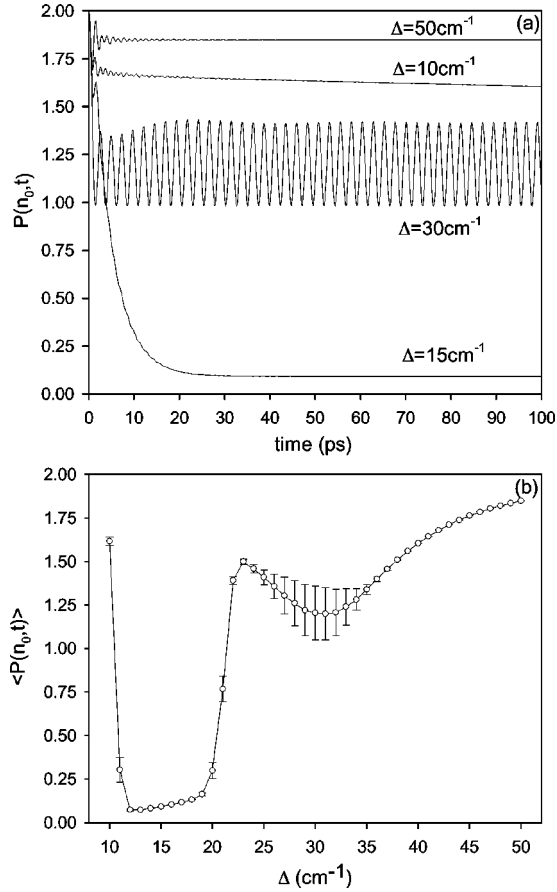
FIG. 3. (a) Defect vibrational population vs time for different Δ values and for $J=3$ cm^{-1}, $A=15$ cm^{-1}, and $N=131$. (b) Average and fluctuations of the defect population vs Δ. The average is performed between 40 and 100 ps.

$$p(n,t) = \sum_{n_1=1}^{n} |\Psi(n_1,n,t)|^2 + \sum_{n_2=n}^{N} |\Psi(n,n_2,t)|^2. \qquad (8)$$

In Fig. 3(a), the evolution of the defect population $p(n_0,t)$ versus time is shown for different Δ values. The anharmonicity and the hopping constant are equal to $A=15$ cm^{-1} and $J=3$ cm^{-1}, respectively, and the lattice size is set to $N=131$. The figure clearly shows the occurrence of different behaviors depending on the strength of the frequency shift. For a strong shift, i.e., $\Delta=50$ cm^{-1}, the population exhibits two regimes. Indeed, in the short time limit, the population first decreases from its initial value equal to 2 and exhibits fast damped oscillations with a period about 1.4 ps. Then, the oscillations disappear and the population reaches an almost constant value equal to 1.85. In other words, 92.5% of the vibrational energy is localized on the defect. For a rather small frequency shift, i.e., $\Delta=10$ cm^{-1}, the defect population shows a similar behavior. Nevertheless, the almost constant value reached in the long time limit is equal to 1.60 so that 80% of the energy is localized on the defect. By contrast, when $\Delta=30$ cm^{-1}, the defect population exhibits undamped oscillations in the long time limit. The period of these oscillations is equal to 2.4 ps and the corresponding frequency is equal to 13.8 cm^{-1}. Note that this permanent regime takes

place after about 20 ps. The defect population evolves between 1.0 and 1.4 so that the average amount of energy localized on the defect is about 60%. Finally, when $\Delta=15$ cm^{-1}, the defect population behaves in a fully different way. Indeed, after exhibiting fast damped oscillations, the population drastically descreases according to an exponential law with a decay rate about 1.07 cm^{-1}. Note that this decay rate γ is obtained by fitting the defect population according to $p(n_0,t)=a+b \exp(-\gamma t)$. After 30 ps, it reaches a constant value equal to 0.09 so that 95.5% of the initially localized energy have left the defect.

To clarify the previous features, Fig. 3(b) represents the average value of the defect population as a function of the frequency shift Δ. Note that the figure also shows the fluctuations of the population around its average value. For a strong frequency shift, i.e., $\Delta=50$ cm^{-1}, the average population is important whereas the fluctuations almost vanish. This feature indicates a rather strong localization of the two vibrons onto the defect site. When Δ decreases, the average population decreases and the fluctuations slowly increase. When the shift reaches the region around $\Delta=30$ cm^{-1}, the average population reaches a minimum value equal to 1.20 whereas the fluctuations are maximum. Such a behavior occurs when Δ ranges typically between 25 and 35 cm^{-1} and indicates the occurrence of oscillations in the defect population. However, by decreasing again the frequency shift, the average population now increases to reach a maximum value equal to 1.5 when $\Delta=23$ cm^{-1}. In that case, the fluctuations have disappeared. Then, when Δ reaches the region located around 15 cm^{-1}, the average population strongly decreases to reach 0.07 and the population does not exhibit any fluctuation. Such a behavior occurs when Δ ranges typically between 12 and 18 cm^{-1} and indicates that the two vibrons have left the defect. Finally, when Δ decreases again, the average population increases again.

The time evolution of the population of the different lattice sites is shown in Figs. 4. When $\Delta=15$ cm^{-1} [Fig. 4(a)], the exponential decay of the defect population is accompanied by the propagation of the vibrational energy along the lattice. Indeed, as the defect population decreases, two population wave packets are emitted on each side of the defect with a velocity about one site per ps. Nevertheless, a part of the vibrational energy stays localized on the defect. When $\Delta=30$ cm^{-1}, the site population is displayed in Fig. 4(b). Although the results concerning the oscillations of the defect population are recovered, the figure shows that the population of the neighboring sites of the defect exhibits oscillations, but with smaller amplitudes. In that case, the main part of the vibrational energy is trapped over a few sites around the defect according to a solution which is spatially localized and time periodic. Note that the emission of a few parts of the energy takes place so that small amplitude population wave packets propagate on each site of the defect. Finally, when $\Delta=50$ cm^{-1}, Fig. 4(c) clearly shows that the main part of the energy is localized on the defect although a very small part of the energy is emitted along the lattice.

Let us now focus our attention on the exponential decay of the defect population. In Fig. 5, the defect population vs time is shown when $J=2.5$ cm^{-1} and $\Delta=A=15$ cm^{-1} (full line), $\Delta=A=20$ cm^{-1} (dashed line), and $\Delta=A=25$ cm^{-1} (dot-
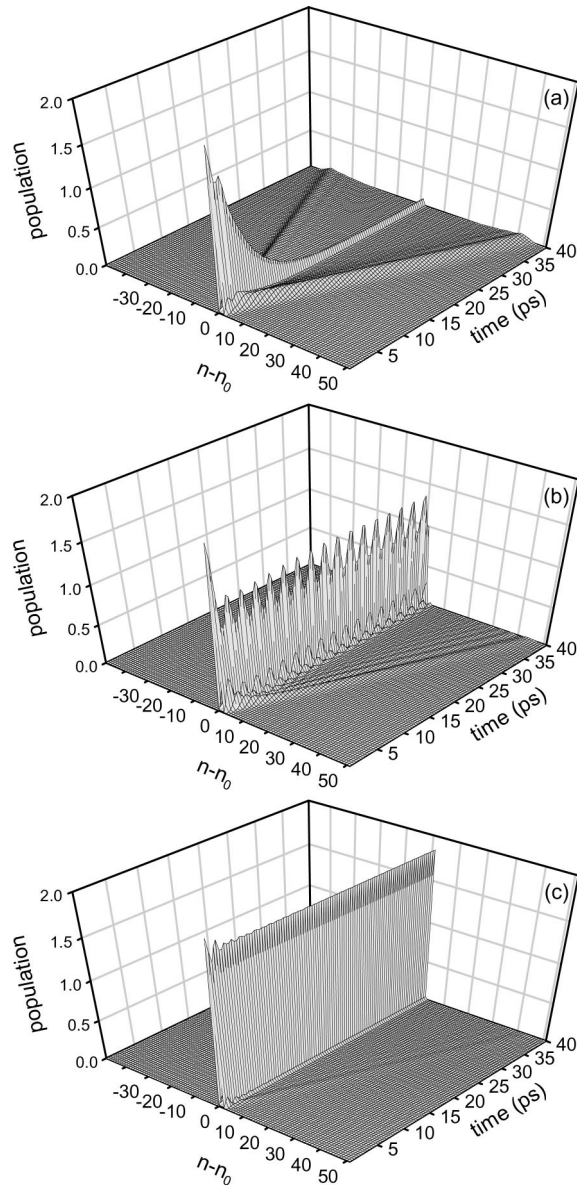
FIG. 4. Vibrational populations vs time for (a) $\Delta=15$ cm^{-1}, (b) $\Delta=30$ cm^{-1}, and (c) $\Delta=50$ cm^{-1}. The anharmonicity is equal to $A=15$ cm^{-1}, the hopping constant is set to $J=3$ cm^{-1}, and the lattice size is equal to $N=131$.

ted line). The figure clearly shows that the exponential decay takes place when $\Delta=A$. As the frequency shift increases, both the decay rate and the amount of localized energy in the long time limit decrease. For instance, the decay rate is equal to 0.69 cm^{-1} when $\Delta=A=15$ cm^{-1} whereas it is equal to 0.44 cm^{-1} when $\Delta=A=20$ cm^{-1} and finally reaches 0.3 cm^{-1} when $\Delta=A=25$ cm^{-1}. Note that the decay rate seems to increase as J increases since it was found to be 1.07 cm^{-1} when $J=3$ cm^{-1} and $\Delta=A=15$ cm^{-1} [Fig. 3(a)].

In Figs. 6, the square modulus of the two-vibron wave function is represented on the 2D equivalent lattice for $t=10$ ps [Fig. 6(a)], $t=20$ ps [Fig. 6(b)], $t=30$ ps [Fig. 6(c)] and $t=40$ ps [Fig. 6(d)]. The parameters used for this simulation are $\Delta=A=15$ cm^{-1} and $J=3$ cm^{-1}. The figures show that the excitation of the defect site at $t=0$ is accompanied by

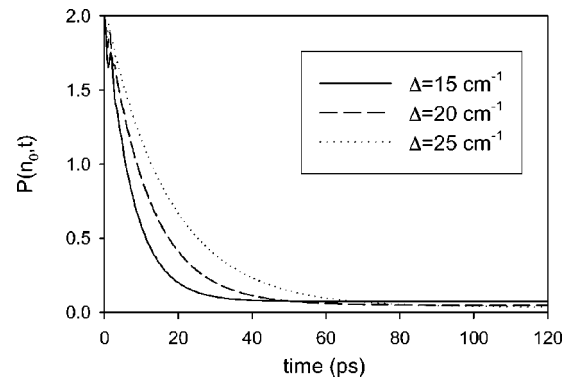FIG. 5. Defect vibrational population vs time for $J=2.5$ cm^{-1} and for $A=\Delta=15$ cm^{-1} (full line), $A=\Delta=20$ cm^{-1} (dashed line), and $A=\Delta=25$ cm^{-1} (dotted line).

the emission of three different wave packets. The wave packet which moves along the direction $n_1=-n_2$ describes two vibrons propagating in the opposite direction on each side of the defect. This feature reveals that the two vibrons initially localized decay in a subspace of the continuum of the two-vibron free states, the subspace connected to two independent vibrons with opposite momenta. Note that the wave packet develops a complex structure as the time increases and spreads out along the line $n_1=-n_2$. In addition, two small wave packets are emitted along the directions $n_1=n_0$ and $n_2=n_0$, respectively. Along the $n_1=n_0$ direction, the wave packet refers to the free propagation of a single vibron on the right side of the defect whereas the other vibron is localized on the defect. Similarly, along the $n_2=n_0$ direction, the wave packet describes the propagation of one vibron on the left side of the defect whereas the other vibron is localized on the defect site. This latter effect corroborates the behavior of the long time limit of the defect population which reaches a nonvanishing constant value.

Finally, in Figs. 7, the behavior of the population of the neighboring sites of the defect is shown when $\Delta=2A=30$ cm^{-1} and $J=3$ cm^{-1}. The time scale has been reduced between 40 and 60 ps so that the features previously observed in Figs. 3(a) and Fig. 4(b) appear more clearly. Figure 7(a) shows that the oscillations of the defect population are accompanied by oscillations in the population of the neighboring sites. All the curves display the same frequency, i.e., about 13.8 cm^{-1}, and the populations of two nearest neighbor sites exhibit oscillations in phase opposition. However, although the defect population oscillates between 1.0 and 1.4, all the other populations vary between zero and a maximum value which decreases as the distance with the defect increases. In Fig. 7(b), the vibron population versus the site position is shown for two typical times. The vibrational population appears strongly localized around the defect and exhibits an exponential decay with respect to the distance with the defect position. However, the figure clearly shows that such a localized object has an internal dynamics similar to a breathing motion. In other words, the vibrational population is not trapped in a conventional localized mode but appears as the quantum counterpart of a well-known classical discrete breather.
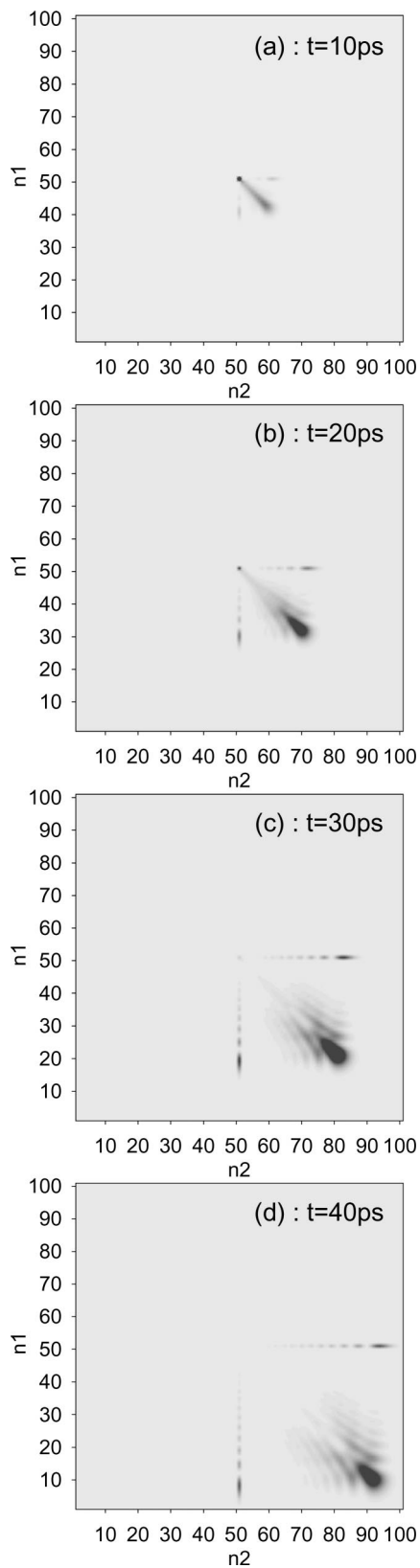
FIG. 6. Representation of the square modulus of the two-vibron wave function on the 2D equivalent lattice for (a) $t=10$ ps, (b) $t=20$ ps, (c) $t=30$ ps, and (d) $t=40$ ps. The parameters used are $J=3$ cm^{-1} and $A=\Delta=15$ cm^{-1}.

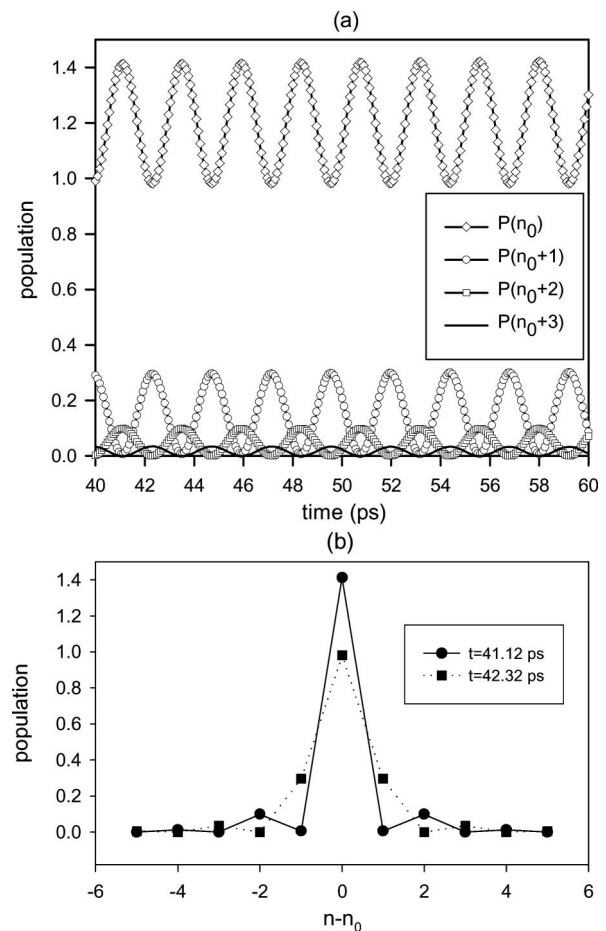FIG. 7. Vibrational population for $J=3$ cm^{-1}, $\Delta=30$ cm^{-1}, and $A=15$ cm^{-1}. (a) Population vs time for the defect site and its neighboring sites. (b) Vibrational population vs the site positions for $t=41.12$ ps (full circles) and $t=42.32$ ps (full squares).

IV. INTERPRETATION AND DISCUSSION

A. General features and Green's function calculation

The previous numerical results clearly show that the presence of a defect in the nanowire strongly modifies the two-vibron dynamics. Indeed, the defect breaks the translational invariance and favors the occurrence of a localized two-vibron bound state (LTVBS) in which the two quanta are trapped on the defect site. The vibrational population of the defect tends to a significant value which appears time independent in the long time limit.

However, singular behaviors take place when the defect frequency shift reaches regions located around both A and $2A$. More precisely, when Δ is close to the anharmonicity A, Fig. 2 shows that a resonance between the LTVBS and the TVFS continuum occurs. The two vibrons initially located on the defect tend to decay on the TVFS continuum. The defect population exhibits an exponential decay and two population wave packets are created and propagate on each side of the defect. By contrast, when the defect frequency shift is twice the anharmonicity, a resonance between the LTVBS and the LSVS+SVFS continuum takes place (see Fig. 2). In that case, a spatially localized and time period

object is created corresponding to the trapping of the two vibrons on few sites around the defect. As in a classical breather, the vibrational populations exhibit oscillations around average values which decrease exponentially as the distance with the defect increases.

Understanding these features requires a perfect description of the two-vibron dynamics through the resolution of the corresponding time dependent Schrodinger equation. This can be achieved either in the time domain or in the frequency domain by applying the well-known evolution operator method. Within this method, the two-vibron state at time t is expressed in terms of the initial state at time $t=0$ as

$$|\Psi(t)\rangle = \mp \int_{-\infty}^{+\infty} \frac{d\omega}{2\pi} 2 \, \text{Im} \, G(\omega \pm i0^+)|\Psi(0)\rangle e^{-i\omega t}, \quad (9)$$

where $G(\omega)$ denotes the two-vibron Green's operator defined as

$$G(\omega) = (\omega - H)^{-1}. \quad (10)$$

To calculate the two-vibron Green's operator, the two-vibron subspace represented by the 2D equivalent lattice is partitioned in five sublattices S_i, $i=0, 1, \ldots, 4$ (see Fig. 1). The sublattice S_0 reduces to the single site $n_1=n_2=n_0$ which describes the two vibrons localized on the defect. The sublattice S_1, formed by the two chains $n_1<n_2=n_0$ and $n_1=n_0<n_2$, corresponds to the LSVS+SVFS continuum. The sublattice S_2 is the square lattice containing the sites $n_1<n_0<n_2$ which describes the TVFS subspace connected to two independent vibrons on each side of the defect. Two vibrons on the same side of the defect are characterized by the sublattice S_3 formed by the two domains $n_1<n_2<n_0$ and $n_0<n_1<n_2$. Finally, the sublattice S_4, formed by the two chains $n_1=n_2 \neq n_0$, corresponds to TVBS.

In that context, the vibron Hamiltonian can be expressed as

$$H = \sum_i H_i + \sum_{i \neq j} V_{ij}, \quad (11)$$

where $H_i=P_iHP_i$ and $V_{ij}=P_iHP_j$ and where P_i denotes the projector on the sublattice S_i. Note that the coupling V_{ij} connects the different sublattices according to the links displayed in Fig. 1.

Since the two vibrons are initially located on the defect, the evolution equation, Eq. (9), can be solved from the knowledge of the projections $G_{i0}=P_iGP_0$, only. Therefore, it is straightforward to show that these projections satisfy the following system of equations:

$$(\omega - H_0)G_{00} - V_{01}G_{10} = P_0,$$

$$(\omega - H_1)G_{10} - \Sigma_{i \neq 1}V_{1i}G_{i0} = 0,$$

$$(\omega - H_2)G_{20} - V_{21}G_{10} = 0,$$

$$(\omega - H_3)G_{30} - V_{31}G_{10} - V_{34}G_{40} = 0,$$

$$(\omega - H_4)G_{40} - V_{41}G_{10} - V_{43}G_{30} = 0. \quad (12)$$

Although Eq. (12) can be solved easily to obtain the required Green's operator, a complete understanding of the numerical results can be achieved from the knowledge of the projection G_{00}, only. This projection characterizes the probability amplitude to find the two vibrons on the defect at time t and is, therefore, strongly connected to the vibrational population of the defect. After performing some algebraic manipulations, this projection is expressed as

$$G_{00}(\omega) = P_0(\omega - H_0 - \Sigma_0(\omega))^{-1}P_0, \quad (13)$$

where the self-energy Σ_0 is defined

$$\Sigma_0(\omega) = V_{01}(\omega - H_1 - \Sigma_1(\omega))^{-1}V_{10}. \quad (14)$$

The self-energy Σ_0 represents the correction of the Hamiltonian H_0 due to the interaction between S_0 and S_1 (see Fig. 1). It is expressed in terms of the corrected Green's operator of the sublattice S_1, i.e. $\tilde{\mathcal{G}}_1(\omega)=(\omega-H_1-\Sigma_1(\omega))^{-1}$, in which the self-energy Σ_1 characterizes the correction of H_1 due to the coupling between S_1 and all the other sublattices. It is expressed as

$$\Sigma_1(\omega) = V_{13}(1 - \mathcal{G}_3 V_{34} \mathcal{G}_4 V_{43})^{-1}\mathcal{G}_3(V_{31} + V_{34}\mathcal{G}_4 V_{41}) + V_{14}(1$$
$$- \mathcal{G}_4 V_{43}\mathcal{G}_3 V_{34})^{-1}\mathcal{G}_4(V_{41} + V_{43}\mathcal{G}_3 V_{31}) + V_{12}\mathcal{G}_2 V_{21}, \quad (15)$$

where $\mathcal{G}_i(\omega)=P_i(\omega-H_i)^{-1}P_i$ stands for the unperturbed Green's operator connected to the sublattice S_i.

The behavior of the projected Green's operator G_{00} is governed by the self-energy Σ_0. Although this quantity cannot be calculated exactly, approximated values can be obtained, especially when the defect frequency shift reaches regions located around A and $2A$. These calculations are illustrated in the following sections.

B. Resonance between LTVBS and TVFS

When the value of the defect frequency shift Δ is close to the anharmonic parameter A, the energy of the LTVBS is resonant with the TVFS continuum. Therefore, to simplify our discussion, we assume that these two kinds of states are isolated from the other two-vibron states. In other words, LSVS+SVFS and TVBS are supposed to lie, respectively, above and below the TVFS. Note that when $\Delta \approx A$, this assumption requires to have an intramolecular anharmonicity greater than the single vibron bandwidth, and appears reasonable for a low-dimensional molecular adsorbate.

In that context, the effective Green's operator $\tilde{\mathcal{G}}_1(\omega)$ of the sublattice S_1, involved in the definition of the self-energy Σ_0 [Eq. (14)], does not exhibit any resonance in the frequency range of the TVFS continuum. As a result, it corresponds to a localized propagator so that the sublattice S_1 can be restricted to its two side sites $\alpha=(n_0,n_0+1)$ and $\beta=(n_0-1,n_0)$ to describe its coupling with the sublattice S_0. The self-energy Σ_0 is thus expressed as

$$\Sigma_0(\omega) \approx 2J^2(\widetilde{\mathcal{G}}_{1\alpha\alpha} + \widetilde{\mathcal{G}}_{1\alpha\beta} + \widetilde{\mathcal{G}}_{1\beta\alpha} + \widetilde{\mathcal{G}}_{1\beta\beta}). \qquad (16)$$

Within this restriction, Fig. 1 shows that the two side sites of the sublattice S_1 are coupled to both sublattices S_2 and S_4. However, in the frequency range of the TVFS continuum, only the coupling between S_1 and S_2 contributes significantly to the self-energy Σ_1 so that $\Sigma_1 \approx V_{12}\mathcal{G}_2 V_{21}$ [Eq. (15)]. Therefore, within the subspace (α, β) of the two side sites, the effective Green's operator $\widetilde{\mathcal{G}}_1$ reduces to the (2×2) matrix expressed as

$$\begin{pmatrix} \omega - 2\omega_0 - \Delta - J^2\mathcal{G}_{2\gamma\gamma} & -J^2\mathcal{G}_{2\gamma\gamma} \\ -J^2\mathcal{G}_{2\gamma\gamma} & \omega - 2\omega_0 - \Delta - J^2\mathcal{G}_{2\gamma\gamma} \end{pmatrix}^{-1},$$

$$(17)$$

where $\mathcal{G}_{2\gamma\gamma}$ defines the diagonal element in the site $\gamma = (n_0-1, n_0+1)$ of the unperturbed Green's operator of the sublattice S_2. Note that since S_2 represents a 2D square lattice, the corresponding Green's function can be computed easily. At this step, by inserting Eq. (17) into Eq. (16), it is straightforward to show that the Green's operator G_{00} is expressed as

$$G_{00}(\omega) = \frac{1}{\omega - 2\omega_0 - 2(\Delta - A) - \Sigma_0(\omega)}, \qquad (18)$$

where the self-energy Σ_0 is defined as

$$\Sigma_0(\omega) = \frac{4J^2}{\omega - 2\omega_0 - \Delta - 2J^2\mathcal{G}_{2\gamma\gamma}(\omega)}. \qquad (19)$$

To illustrate the behavior of the projection G_{00}, the response function $-2\,\mathrm{Im}\,G_{00}(\omega + i0^+)$, corresponding to the Fourier transform of the evolution operator [Eq. (9)], is shown in Fig. 8(a) for $A = 20$ cm^{-1}, $J = 2.5$ cm^{-1} and for $\Delta = 18$, 20, and 22 cm^{-1}. The response function exhibits a single peak in the frequency range of the TVFS continuum which both the position and the width strongly depend on the defect frequency shift Δ. The peak position is blueshifted as Δ increases and the linewidth, given by the imaginary part of the self-energy $-\mathrm{Im}\,\Sigma_0(\omega + i0^+)$, decreases as Δ increases [Fig. 8(b)]. This linewidth depends on the frequency and exhibits a maximum value at the center of the TVFS continuum whereas it almost vanishes at the sides of that continuum.

As displayed in Fig. 8(a), the response function shows an almost Lorentzian lineshape in which both the lineposition and the linewidth can be characterized by neglecting the frequency dependence of the self-energy $\Sigma_0(\omega)$. Therefore, according to the result displayed in Fig. 8(b), the self-energy is approximated by its value at the center of the TVFS continuum so that $\Sigma_0(\omega + i0^+) \approx \Sigma_0(2\omega_0 + i0^+) = \delta - i\Gamma$. Moreover, at the center of the TVFS continuum, it is straightforward to show that the unperturbed Green's operator of the square sublattice S_2 has no real part and is expressed as $\mathcal{G}_{2\gamma\gamma}(2\omega_0 + i0^+) = -8i/3\pi J$. Therefore, from Eq. (19), the parameters δ and Γ are written as

$$\Gamma = \frac{16}{3\pi} \frac{J}{\left(\frac{\Delta}{2J}\right)^2 + \left(\frac{8}{3\pi}\right)^2},$$
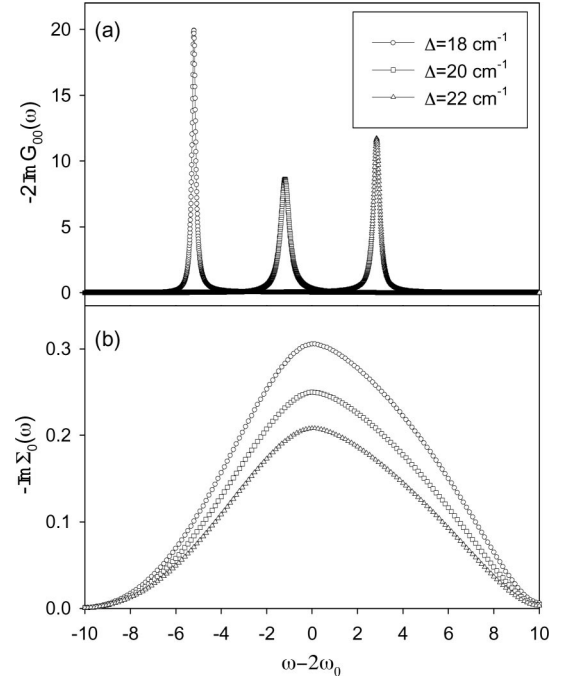

FIG. 8. (a) Imaginary part of the LTVBS Green's function for $J = 2.5$ cm^{-1}, $A = 20$ cm^{-1}, and for $\Delta = 18$ cm^{-1} (circles), $\Delta = 20$ cm^{-1} (squares), and $\Delta = 22$ cm^{-1} (triangles). (b) Imaginary part of the LTVBS self-energy.

$$\delta = -\frac{\Delta}{\left(\frac{\Delta}{2J}\right)^2 + \left(\frac{8}{3\pi}\right)^2}. \qquad (20)$$

At this step, by inserting Eq. (20) into Eq. (18) and by integrating Eq. (9), the wave function connected to the two vibrons located on the defect is expressed as

$$\Psi(n_0, n_0, t) = e^{-i(2\omega_0 + 2(\Delta - A) + \delta)t} e^{-\Gamma t}. \qquad (21)$$

Since the propagation along the sublattice S_1 is negligible, the vibrational population of the defect, Eq. (8), is finally written as

$$p(n_0, t) \approx 2e^{-2\Gamma t}. \qquad (22)$$

In perfect agreement with our numerical simulations, the previous theoretical approach shows that the exponential decay of the defect population results from the indirect coupling between the LTVBS and the TVFS mediated by intermediate states located in the LSVS+SVFS continuum. Indeed, the LTVBS experiences nonresonant interactions with states corresponding to the localization of the first vibron on the defect whereas the second vibron is located either on the left side or on the right side of the defect. Such states can evolve according to three different ways leading to the full delocalization of the second vibron, to the trapping of the first vibron on the second vibron, and to the delocalization of the first vibron in the opposite direction of the second vibron. This latter process is the main mechanism when the resonant condition $\Delta \approx A$ is satisfied. As a consequence, the LTVBS decays on the subspace S_2 of the TVFS continuum corresponding to two independent vibrons propagating in an opposite direction on each side of the defect. Note that the

two independent vibrons are emitted according to an entangled state due to their indistinguishable nature. The Lorentzian lineshape of the response function shows that the TVFS involved in the process are those centered around the frequency $2\omega_0 + 2(\Delta - A) + \delta$ over a frequency range of about 2Γ.

As shown in Eq. (20), the decay rate Γ decreases as the defect frequency shift Δ increases and it increases with the hopping constant J. This behavior characterizes the fact that the strength of the coupling between the LTVBS and the intermediate LSVS+SVFS continuum is proportional to the hopping constant J whereas it decreases as the energy difference between the two kinds of states, proportional to Δ, increases. Note that when $J = 2.5$ cm^{-1}, the decay rate 2Γ for the defect population is equal to 0.87, 0.50, and 0.33 cm^{-1} when $\Delta = 15$, 20, and 25 cm^{-1}, respectively, in rather good agreement with the numerical values discussed in Sec. III. To conclude this section, let us mention that the propagation along the sublattice S_1 has been neglected in the present approach. However, because the intermediate LSVS+SVFS participate in the LTVBS decay, the probability for such a propagation, even small due to the nonresonant nature of the intermediate states, does not vanish exactly. As a consequence, a few parts of the vibrational energy stays localized on the defect so that the defect population does not strictly tend to zero in the long time limit.

C. Resonance between LTVBS and LSVS+SVFS

When the value of the defect frequency shift Δ is close to $2A$, the energy of the LTVBS is resonant with the LSVS+SVFS continuum (see Fig. 2). As previously, to simplify our discussion, we assume that these two kinds of states are isolated from the other two-vibron states so that both TVFS and TVBS are supposed to lie below the LSVS+SVFS.

In that context, Eq. (15) clearly shows that all the interactions defining the self-energy of the sublattice S_1 involve nonresonant states. As a consequence, we assume the self-energy Σ_1 negligible so that the corrected Green's operator $\tilde{\mathcal{G}}_1$ can be approximated by the corresponding unperturbed Green's operator $\mathcal{G}_1$. The self-energy connected to the LTVBS [Eq. (14)] is thus expressed as

$$\Sigma_0(\omega) = 2J^2(\mathcal{G}_{1\alpha\alpha} + \mathcal{G}_{1\beta\beta}). \tag{23}$$

In others words, by neglecting the interactions between S_1 and all the sublattices S_i, $i \neq 0$, the 2D equivalent lattice describing the two vibron dynamics reduces to a linear chain formed by the two sublattices S_0 and S_1. The discrete state LTVBS represented by the single site S_0 is thus coupled to the side sites α and β of the two semi-infinite chains defining the sublattice S_1. Within this picture, the procedure introduced by Dobrzynski[32] to calculate the response function of superlattices and composite materials can be applied and it is straightforward to show that the Green's function $\mathcal{G}_{1\alpha\alpha}$ is expressed as

$$\mathcal{G}_{1\alpha\alpha}(\omega) = \frac{\frac{\omega - 2\omega_0 - \Delta}{2J} \pm \sqrt{\left(\frac{\omega - 2\omega_0 - \Delta}{2J}\right)^2 - 1}}{J}, \tag{24}$$

where the sign $\pm$ is chosen to ensure the regularity of the Green's function at the infinity. Therefore, since $\mathcal{G}_{1\beta\beta} = \mathcal{G}_{1\alpha\alpha}$ by symmetry, the self-energy Σ_0 [Eq. (23)] can be calculated easily and the Green's operator projected on the LTVBS, Eq. (13), is finally written as

$$G_{00}(\omega) = \frac{1}{2JD(\theta)} \begin{cases} \theta + \eta + 2\sqrt{\theta^2 - 1}, & \text{if } \theta > 1; \\ \theta + \eta + 2i\sqrt{1 - \theta^2}, & \text{if } |\theta| < 1; \\ \theta + \eta - 2\sqrt{\theta^2 - 1}, & \text{if } \theta < -1; \end{cases} \tag{25}$$

where the reduced parameters $\theta = (\omega - 2\omega_0 - \Delta)/2J$ and $\eta = (\Delta - 2A)/2J$ have been introduced and where $D(\theta) = 3\theta^2 - 2\eta\theta - \eta^2 - 4$. Equation (25) shows that the behavior of the projected Green's operator depends on whether the frequency ω lies inside the LSVS+SVFS energy band or not. As a result, the response function, $-2\,\mathrm{Im}\,G_{00}(\omega + i0^+)$, is the sum of three contributions as

$$\begin{aligned} -2\,\mathrm{Im}\,G_{00}(\omega + i0^+) = &-\frac{2}{3J}\frac{\sqrt{1-\theta^2}}{(\theta - \theta_+)(\theta - \theta_-)}(h(\theta + 1) \\ &- h(\theta - 1)) + \frac{\pi}{3J}\left(1 - \frac{2\eta}{\sqrt{\eta^2 + 3}}\right) \\ &\times \delta(\theta - \theta_-)(1 - h(\eta - 1)) \\ &+ \frac{\pi}{3J}\left(1 + \frac{2\eta}{\sqrt{\eta^2 + 3}}\right)\delta(\theta - \theta_+)h(\eta + 1), \end{aligned} \tag{26}$$

where $h(x)$ denotes the Heavisde step function and where $\theta_\pm$, which are the zeros of the function $D(\theta)$, represent the poles of the Green's function as

$$\theta_\pm = \frac{\eta}{3} \pm \frac{2}{3}\sqrt{\eta^2 + 3}. \tag{27}$$

As illustrated in Fig. 9(a) for $J = 2$ cm^{-1} and $\Delta = 2A = 40$ cm^{-1}, the response function, Eq. (26), exhibits a nonvanishing continuous part in the frequency range of the LSVS+SVFS band which extends from $\omega = 2\omega_0 + \Delta - 2J$ (i.e., $\theta = -1$) to $\omega = 2\omega_0 + \Delta + 2J$ (i.e., $\theta = 1$). In addition, the response function shows two delta peaks located, respectively, below and above the band. These two peaks occur at the frequencies of the two poles $\theta_\pm$ of the Green's function defined in Eq. (27). As displayed in Fig. 9(b), the shape of the continuous part depends on the Δ values. For instance, although it is almost uniform when $\Delta = 2A$, the response increases in the vicinity of the low frequency band edge as Δ increases to develop a divergence when $\Delta = 2A + 2J$, i.e., when $\eta = 1$. However, as increasing Δ again, the divergence finally disappears. The same behavior takes place at the high frequency band edge when Δ decreases and a divergence occurs when $\Delta = 2A - 2J$ (i.e., when $\eta = -1$). As shown in Figs. 10, this behavior is strongly correlated to the evolution of the two poles of the Green's function. Figure 10(a) dis-
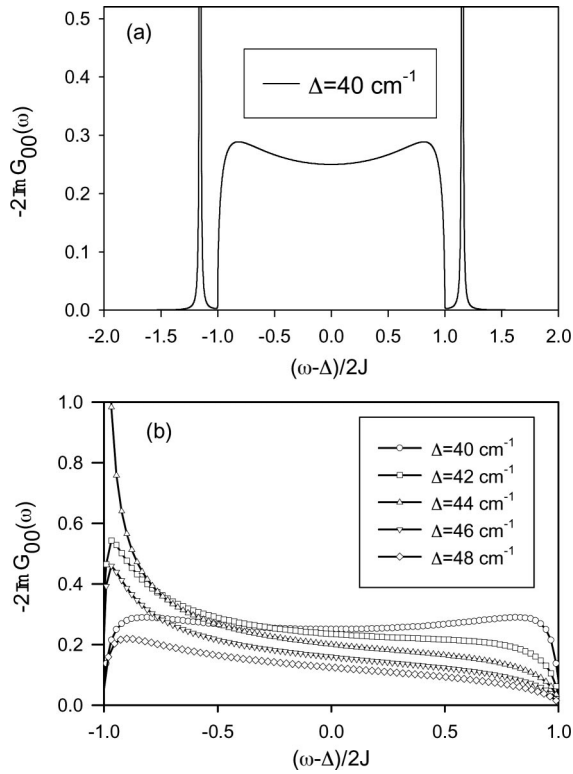
FIG. 9. (a) Imaginary part of the LTVBS Green's function for $J=2$ cm^{-1}, $A=20$ cm^{-1}, and $\Delta=40$ cm^{-1}. (b) Representation in the frequency range of the LSVS+SVFS continuum for different Δ values. Note that ω_0 has been used as the origin of the frequency so that $\omega_0=0$.
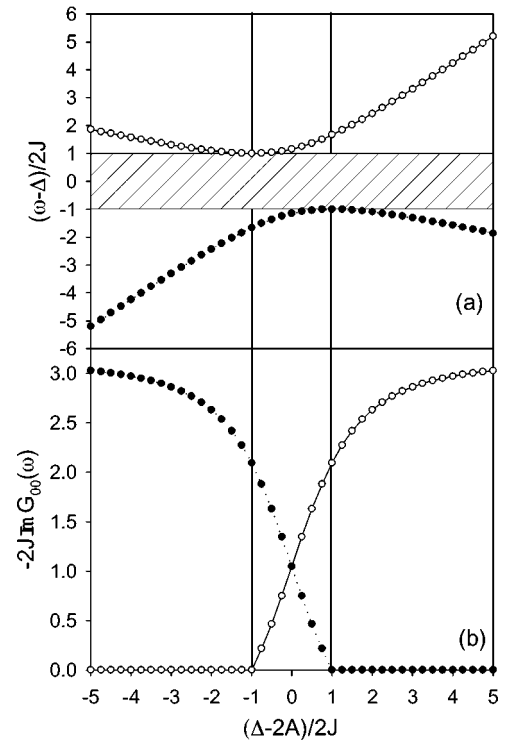

FIG. 10. (a) Position and (b) amplitude of the high frequency (open circles) and low frequency (full circles) peaks of the imaginary part of the LTVBS Green's function vs the η parameter (see the text).

plays the frequency of the delta peaks versus the reduced parameter η whereas Fig. 10(b) shows the intensity of the delta peaks. It is shown that the low frequency peak occurs when $\eta<1$, i.e., when $\Delta-2A<2J$, whereas the high frequency peak takes place when $\eta>-1$, i.e., when $\Delta-2A>-2J$. As a result, the two peaks occur simultaneously when $-1<\eta<1$, only. Note that the disappearance of a delta peak corresponds to a divergence in the continuous part of the response.

To understand the behavior of the response function, let us remain that when Δ is close to $2A$, the 2D equivalent lattice reduces to a 1D chain formed by the combination of the two sublattices S_0 and S_1 (see Fig. 1). In terms of two vibron states, this chain describes the trapping of a vibron on the defect whereas the other vibron is allowed to propagate along the nanowire. The chain exhibits two kinds of defects. First, the frequency of the site S_0, equal to $2\omega_0+2(\Delta-A)$, differs from the frequency of the sites of the sublattice S_1, equal $2\omega_0+\Delta$. Then, two defects correspond to a singularity in the hopping constant, equal to $\sqrt{2}J$, between S_0 and the two side sites of the sublattice S_1. From a physical point of view, these defects in the equivalent lattice originate from the fact that when a vibron is trapped on the real defect, it modifies the dynamics of the other vibron in the vicinity of this latter defect. Due to the intramolecular anharmonicity, it is first responsible for a frequency shift when the two vibrons are localized on the defect. Then, it enhances the hopping constant of the process involving the hop of the other vibron on the defect site.

In that context, the presence of defects in the equivalent 1D chain is responsible for the occurrence of both extended states and localized states, for the fictitious particle. The extended states, which belong to the energy band defined by the sublattice S_1, are responsible for the continuous part of the response function. They correspond to states in which a vibron is trapped on the defect whereas the other vibron is fully delocalized along the nanowire. In addition, it is straightforward to show that the 1D chain supports localized states which produce the delta peaks in the response function. These states, which the frequencies are specified by the poles of the Green's function, are strongly localized on the site S_0. However, the number of localized states depends on whether the LTVBS lies in the LSVS+SVFS band or not, as a result of the competition between the two kinds of defects in the 1D chain. When the LTVBS is located in the band, two localized states occur essentially due to the singularity of the hopping process in the vicinity of the defect. By contrast, when the LTVBS lies above ($\eta>1$) or below ($\eta<-1$) the band, a single localized state remains due to the influence of the intramolecular anharmonicity. In both cases, a localized state corresponds to a bound state in which the two vibrons are trapped around the defect site. These features are illustrated in Fig. 11 which displays the high frequency and the low frequency wave function of the 1D chain for $J=2$ cm^{-1} and $A=20$ cm^{-1}. When $\Delta=2A$ [Fig. 11(a)], the chain exhibits two localized states centered on the site S_0. Although both wave functions exhibit an exponential decay, the low frequency state shows spatial oscillations so that two nearest neighbor sites are characterized by amplitudes in
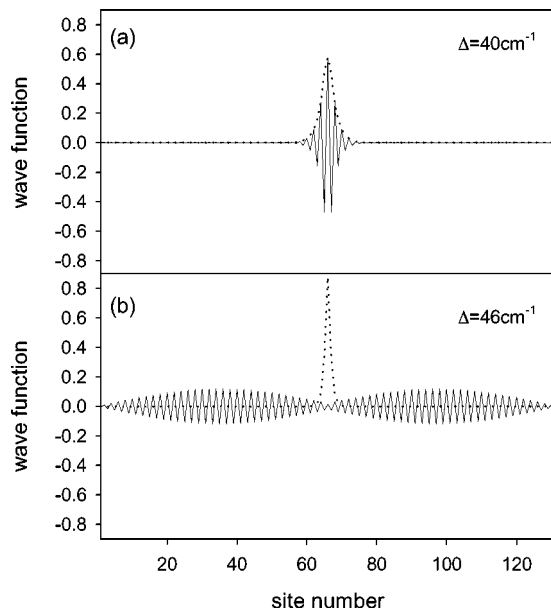
FIG. 11. High frequency (dotted line) and low frequency (full line) wave function for the fictitious particle along the 1D chain formed by the combination of the S_0 and S_1 sublattices for $J=2$ cm^{-1} and $A=20$ cm^{-1}. (a) When $\Delta=40$ cm^1, the chain supports two localized states centered on the site S_0. (b) When $\Delta=46$ cm^1, only the high frequency localized state remains.

phase opposition. When $\Delta=2A+4J$ [Fig. 11(b)] only the high frequency state remains localized.

At this step, by integrating Eq. (9) from the knowledge of the response function, Eq. (26), the wave function connected to the two vibrons located on the defect is expressed as

$$\Psi(n_0,n_0,t) = \Psi_c(n_0,n_0,t)$$
$$+ e^{-i(2\omega_0+\Delta+2J\theta_-)t}\left[1-\frac{2\eta}{\sqrt{\eta^2+3}}\right]\frac{1-h(\eta-1)}{3}$$
$$+ e^{-i(2\omega_0+\Delta+2J\theta_+)t}\left[1+\frac{2\eta}{\sqrt{\eta^2+3}}\right]\frac{h(\eta+1)}{3},$$
$$(28)$$

where $\Psi_c(n_0,n_0,t)$ denotes the contribution of the response function in the frequency range of the LSVS+SVFS band. In the long time limit, such a contribution vanishes. Indeed, it is straightforward to show that when the continuous part of the response is almost uniform, the integration of Eq. (9) over the LSVS+SVFS band leads to $\Psi_c(n_0,n_0,t)\approx\sin(2Jt)/2Jt$. By contrast, when a divergence takes place, Eq. (26) shows that the response function behaves as $1/\sqrt{\theta\pm1}$ so that the integration of Eq. (9) over the LSVS+SVFS band leads to $\Psi_c(n_0,n_0,t)\approx1/\sqrt{Jt}$. Therefore, whatever the situation, $\Psi_c(n_0,n_0,t)\to0$ when $Jt\gg1$.

Finally, since the two peaks refer to states strongly localized on the sublattice S_0, the long time limit of the defect population, Eq. (8), is given by $p(n_0,t)\approx1+|\Psi(n_0,n_0,t)|^2$ and is written as

$$p(n_0,t) \approx 1 + \frac{2}{9}\frac{(3+5\eta^2)+(3-3\eta^2)\cos\left(\frac{8J}{3}\sqrt{\eta^2+3}t\right)}{\eta^2+3},$$
$$(29)$$

when $|\eta|<1$ whereas it is expressed as

$$p(n_0,t) \approx 1 + \frac{1}{9}\left[1+\frac{2|\eta|}{\sqrt{\eta^2+3}}\right]^2,$$
$$(30)$$

when $|\eta|>1$.

When $|\eta|<1$, i.e., when the LTVBS lies in the LSVS +SVFS band, the two vibron wave function $\Psi(n_0,n_0,t)$ reduces to the coherent superimposition of the two localized states. As a result, the defect population shows oscillations which the frequency is equal to the frequency difference between the two localized states. In particular, at the resonance $\eta=0$, i.e., when $\Delta=2A$, the defect population oscillates between 1 and $1+4/9=1.44$ according to the frequency $8J/\sqrt{3}$ equal to 13.85 cm^{-1} when $J=3$ cm^{-1}. These results are in perfect agreement with the numerical results shown in Figs. 3, 4, and 7 (see Sec. III). Note that the spatial dependence of the two localized states [Fig. 11(a)] is responsible for the fact that the population between two nearest neighbor sites appears in phase opposition. By contrast, when $|\eta|>1$, a single localized state remains so that the defect population appears time independent. Note that when $J=3$ cm^{-1}, $A=15$ cm^{-1}, and $\Delta=50$ cm^{-1}, Eq. (30) leads to a defect population equal to 1.85 in perfect agreement with the numerical results displayed in Figs. 3 and 4.

D. Conclusion

In this paper, it has been shown that the presence of a local defect in a molecular nanowire strongly modified the two-vibron dynamics. Indeed, the defect breaks the translational invariance and favors the occurrence of a localized two-vibron bound state (LTVBS) in which the two quanta are trapped on the defect site. However, the numerical integration of the time dependent two-vibron Schrodinger equation with two vibrons initially located on the defect has revealed the occurrence of two singular behaviors.

When the defect frequency shift Δ is close to the anharmonicity A, a resonance between the LTVBS and the TVFS takes place mediated by nonresonant intermediate states located in the LSVS+SVFS continuum. As a result, the two vibrons initially located on the defect decay on the subspace of the TVFS continuum corresponding to two independent vibrons propagating in the opposite direction. In other words, the resonance breaks the localized vibron pair and two independent vibrons are emitted on each side of the defect. By contrast, when the defect frequency shift is almost twice the anharmonicity, a resonance between the LTVBS and the LSVS+SVFS occurs. In that case, it has been shown that a vibron trapped on the defect modifies the dynamics of the second vibron. When the LTVBS lies in the LSVS+SVFS band, the trapped vibron essentially enhances the hopping constant experienced by the second vibron when this latter one realizes a hop on the defect. As a result, two localized states occur in which the two vibrons are trapped over few

sites around the defect. Starting with two vibrons on the defect, the wave function evolves in time and converges to a coherent superimposition of these two localized states. A spatially localized and time period object is created in which the vibrational populations exhibit oscillations around average values which decrease exponentially as the distance with the defect increases. When the LTVBS lies outside the LSVS +SVFS band, a single localized state remains essentially due to the intramolecular anharmonicity which is responsible for a frequency shift when the two vibrons are located on the defect. As a result, the vibrational population remains essentially localized on the defect but does not exhibit oscillation anymore.

To conclude, let us mention that this study opens a new way in the elaboration of nanodevices allowing the control of the information storage and transfer at the nanoscale. This feature requires the ability to create two vibrons on the defect and to control their dynamics by playing with the resonances previously described. For instance, such processes can be realized by using simultaneously an infrared laser and a STM. Indeed, by creating a strong frequency shift of the molecule located below the STM, two quanta can be excited on that molecule with an infrared laser which the frequency has been judiciously chosen. The vibrational energy is thus trapped on this molecule until its frequency is shifted to induce a resonance with the TVFS simply by tuning the bias voltage between the STM and the substrate. As a result, the local vibron pair is broken and an energy flow takes place on each side of the defect. The theoretical analysis of such a mechanism is currently in progress and will be addressed in more detail in a forthcoming paper.

*Electronic address: vincent.pouthier@univ-fcomte.fr

[1] A. S. Davydov and N. I. Kisluka, Phys. Status Solidi **59**, 465 (1973); Zh. Eksp. Teor. Fiz. **71**, 1090 (1976) [Sov. Phys. JETP **44**, 571 (1976)].

[2] S. Aubry, Physica D **103**, 201 (1997).

[3] S. Flach and C. R. Willis, Phys. Rep. **295**, 181 (1998).

[4] R. S. MacKay, Physica A **288**, 174 (2000).

[5] A. J. Sievers and S. Takeno, Phys. Rev. Lett. **61**, 970 (1988).

[6] J. C. Kimball, C. Y. Fong, and Y. R. Shen, Phys. Rev. B **23**, 4946 (1981).

[7] F. Bogani, G. Cardini, V. Schettino, and P. L. Tasselli, Phys. Rev. B **42**, 2307 (1990).

[8] A. C. Scott, J. C. Eilbeck, and H. Gilhoj, Physica D **78**, 194 (1994).

[9] V. Pouthier and C. Girardet, Phys. Rev. B **65**, 035414 (2002).

[10] V. Pouthier, J. Chem. Phys. **118**, 3736 (2003).

[11] V. Pouthier, J. Chem. Phys. **118**, 9364 (2003).

[12] V. Pouthier, Phys. Rev. E **68**, 021909 (2003).

[13] V. Pouthier and C. Falvo, Phys. Rev. E **69**, 041906 (2004).

[14] P. Guyot-Sionnest, Phys. Rev. Lett. **67**, 2323 (1991).

[15] R. Honke, P. Jakob, Y. J. Chabal, A. Dvorak, S. Tausendpfund, W. Stigler, P. Pavone, A. P. Mayer, and U. Schröder, Phys. Rev. B **59**, 10996 (1999).

[16] R. P. Chin, X. Blase, Y. R. Shen, and S. GT. Louie, Europhys. Lett. **30**, 399 (1995).

[17] D. J. Dai and G. E. Ewing, Surf. Sci. **312**, 239 (1994).

[18] P. Jakob, Phys. Rev. Lett. **77**, 4229 (1996).

[19] P. Jakob, Physica D **119**, 109 (1998).

[20] P. Jakob, J. Chem. Phys. **114**, 3692 (2001).

[21] P. Jakob, Appl. Phys. A: Mater. Sci. Process. **75**, 45 (2002).

[22] P. Jakob and B. N. J. Persson, J. Chem. Phys. **109**, 8641 (1998).

[23] H. Okuyama, T. Ueda, T. Aruga, and M. Nishijima, Phys. Rev. B **63**, 233404 (2001).

[24] J. Edler, R. Pfister, V. Pouthier, C. Falvo, and P. Hamm, Phys. Rev. Lett. **93**, 106405 (2004).

[25] V. Pouthier, J. C. Light, and C. Girardet, J. Chem. Phys. **114**, 4955 (2001).

[26] C. Falvo and V. Pouthier, J. Chem. Phys. **122**, 014701 (2005).

[27] B. N. J. Persson and Ph. Avouris, Chem. Phys. Lett. **242**, 483 (1995).

[28] B. N. J. Persson and Ph. Avouris, Surf. Sci. **390**, 45 (1997).

[29] H. C. Akpati, P. Nordlander, L. Lou, and Ph. Avouris, Surf. Sci. **372**, 9 (1997).

[30] H. C. Akpati, P. Nordlander, L. Lou, and Ph. Avouris, Surf. Sci. **401**, 47 (1998).

[31] W. H. Press, S. A. Teukolsky, W. T. Vetterling, and B. P. Flannery, *Numerical Recipes in FORTRAN*, 2nd ed. (Cambridge University Press, Cambridge, 1992).

[32] L. Dobrzynski, Surf. Sci. **299/300**, 1008 (1994).